Available online at www.sciencedirect.com
SCIENCE DIRECT
Journal of Solid State Chemistry 179 (2006) 1948–1956
JOURNAL OF SOLID STATE CHEMISTRY
www.elsevier.com/locate/jssc

The crystal structure of the interrupted framework silicate $K_{9.6}Ca_{1.2}Si_{12}O_{30}$ determined from laboratory X-ray diffraction data

V. Kahlenberg[a,*], R. Kaindl[a,b], D.M. Többens[a]

[a]*Institute of Mineralogy and Petrography, University of Innsbruck, Innrain 52, A-6020 Innsbruck, Austria*
[b]*Christian-Doppler-Laboratory for Advanced Hard Coatings at the Institute of Mineralogy and Petrography, University of Innsbruck, Innrain 52, A-6020 Innsbruck, Austria*

Received 6 February 2006; received in revised form 28 March 2006; accepted 31 March 2006
Available online 6 April 2006

Abstract

The crystal structure of a potassium calcium silicate with composition $K_{9.6}Ca_{1.2}Si_{12}O_{30}$ (or $K_8CaSi_{10}O_{25}$) has been solved by direct methods aided by distance least squares optimization from laboratory X-ray powder diffraction data. The trigonal compound adopts the non-centrosymmetric space group $R3c$ with the following basic crystallographic data: $a = 11.13623(5)$ Å, $c = 21.9890(2)$ Å, $V = 2361.63(2)$ Å^3, $Z = 3$, $D_{calc} = 2.617$ g cm^{-3}. The crystal structure can be classified as an interrupted framework with exclusively Q^3-units. It can be thought of as being built from layers parallel to (001) containing isolated six-membered tetrahedral rings in UDUDUD conformation. Corner sharing of tetrahedra belonging to adjacent sheets results in a tetrahedral framework. The framework density of the structure is 15.2 T-atoms/1000 Å^3. The coordination sequences are identical for both silicon atoms in the asymmetric unit: 3-6-11-20-32-46-60-80-102-122. The vertex symbols for the two tetrahedral centers are $10_2 \cdot 10_2 \cdot 6_1$. Topologically, the structure can be described as an Archimedean three-dimensional 3-connected net. It can be derived from the diamond or cristobalite net by removing 20% of the knots. Charge compensation in the structure is achieved by the incorporation of mono- and divalent M-cations (M: K, Ca). These extra-framework ions are coordinated by six to nine oxygen ligands. Ca/K distributions for the five symmetrically independent M-sites were obtained from a combination of bond distance considerations, site occupancy refinements and the bulk chemical composition. The structural characterization is completed by a detailed Raman spectroscopic study. Furthermore, possible implications of the structural chemistry of interrupted framework silicates for the field of silicate glass research are addressed.

Keywords: Ab initio structure determination; Raman spectroscopy

1. Introduction

The ternary system K_2O–CaO–SiO_2 is of interest for several processes and materials related to applied mineralogy including, for example, technical [1] and medieval [2–4] glasses, blast furnace linings [5] and combustion ashes [6]. However, unlike its importance in these fields and, additionally, the frequent occurrence of potassium and calcium oxide in silicate minerals it is surprising that there is only very little information concerning the crystal structures and the structural chemistry of the phases in the system K_2O–CaO–SiO_2. There exist some structural data on hydrated phases including minerals such as rhodesite and hydroxyapophyllite or synthetic CAS-1 [7]. However, to our best knowledge no pure calcium silicate has been structurally characterized so far. This is even more surprising because the phase equilibrium studies on this system performed by Taylor [8] as well as Morey et al. [9] reported the existence of at least eight different ternary phases: $K_2Ca_{23}Si_{12}O_{48}$, $K_2Ca_2Si_9O_{21}$, $K_4CaSi_6O_{15}$, $K_2Ca_2Si_6O_{15}$, $K_2Ca_3Si_6O_{16}$, $K_4CaSi_3O_9$, K_2CaSiO_4 and $K_8CaSi_{10}O_{25}$, respectively. For the last three compounds in this list at least some basic crystallographic data have been published and indexed powder diffraction patterns can be found in the *Powder Diffraction File* (PDF-4). For both, $K_4CaSi_3O_9$ and K_2CaSiO_4, cubic primitive unit cells were reported. From the similarity between the lattice

*Corresponding author. Fax: +43 0 512 507 2926.
E-mail address: volker.kahlenberg@uibk.ac.at (V. Kahlenberg).

0022-4596/$ - see front matter © 2006 Elsevier Inc. All rights reserved.
doi:10.1016/j.jssc.2006.03.044

parameters of $K_4CaSi_3O_9$ and $Na_4CaSi_3O_9$ it was suggested that both phases may be isostructural [10]. For $K_8CaSi_{10}O_{25}$ the same authors proposed a hexagonal R-centered unit cell with $a = 11.125$ Å and $c = 10.987$ Å [10]. Concerning the crystal system to be considered, this result agrees with earlier studies of Morey et al. [9] who reported that $K_8CaSi_{10}O_{25}$ forms optically uniaxial negative crystals.

This investigation is part of a more comprehensive study on the crystal chemistry of potassium calcium silicates and was aimed to characterize the crystal structure of $K_8CaSi_{10}O_{25}$ in more detail. Since our efforts to grow suitable single crystals of this phase were not successful, structure determination was based on laboratory powder diffraction data. In the course of the structure determination it became obvious that the formula $K_8CaSi_{10}O_{25}$ which was proposed in former studies leads to a non-integral number of formula units per cell. Therefore, we finally decided to describe the chemical composition of the present potassium calcium silicate as $K_{9.6}Ca_{1.2}Si_{12}O_{30}$, resulting in the same bulk chemistry. The X-ray diffraction studies are completed by Raman spectroscopical investigations.

2. Experimental section

Starting materials for the preparation of $K_8CaSi_{10}O_{25}$ (or $K_{9.6}Ca_{1.2}Si_{12}O_{30}$) were $CaCO_3$ (Merck, p.a.), K_2CO_3 (AlfaAesar, puratronic) and fine grained (<40 mesh) SiO_2 powder (AlfaAesar, 99.995). Since the compound is known to melt congruently at 946 °C [9], initial synthesis experiments were aimed to obtain single crystalline material. However, these trials were only partially successful. The crystals obtained from (a) slow cooling of the melt as well as (b) devitrification of quenched glasses were too small to be investigated by laboratory single crystal diffraction (<10 μm) and/or showed poor optical (undulous extinction under the polarizing microscope) and diffraction quality. Therefore, we finally decided to perform the structural studies using polycrystalline samples prepared from solid state reactions. One gram of the reagents (in the appropriate molar ratio) was carefully mixed in an agate mortar under acetone and pressed into discs. The pellets confined in closed 50 ml platinum crucibles were fired in air from 200 °C with 5 °C/min to 900 °C in a resistance heated furnace, subsequently held at this temperature for 2 days and finally quenched. The product was characterized by preliminary X-ray powder diffraction. The firing procedure was repeated until no differences between the powder patterns of subsequent cycles could be detected. For the determination of the chemical composition of the sintered pellets, an electron probe microanalysis was performed using a JEOL JXA-8100 Superprobe with a lateral resolution of 1 μm^3 (10 kV, 20 nA). The analysis resulted in the following average chemical composition for ten spots (normalized to 25 oxygen atoms): $K_{7.94(5)}Ca_{1.05(4)}Si_{10.03(4)}O_{25}$. This result is almost identical with the expected cation ratios of K:Ca:Si = 8:1:10 based on the molar ratios of the educts and proves that a potassium-loss due to evaporation during the burning process can be neglected. X-ray powder diffraction data for structure determination and refinement have been collected on a Stoe STADI-MP diffractometer in flat-plate transmission geometry using a sample of 6 mm diameter prepared between two thin foils. The diffractometer is equipped with an asymmetric primary beam Ge(111) monochromator (yielding a strictly monochromatic Cu$K\alpha_1$ radiation) and a linear PSD with 6° detector range. The effective value of 0.79 for the product μt (μ = linear absorption coefficient; t = sample thickness) used for the absorption correction was determined experimentally from the intensity ratios at $\theta = 0°$ with and without the sample. Details of the data collection and the refinement are given in Table 1.

Confocal Raman spectra were obtained with a HORIBA JOBIN YVON LabRam-HR 800 Raman micro-spectrometer. Samples were excited using the 489.8 nm emission line of a 30 mW Ar^+-laser and an OLYMPUS 100× objective (N.A. = 0.9). Size and power of the laser spot on the surface was approximately 1 μm and 5 mW. The spectral resolution, determined by measuring the Rayleigh line, was about 1.8 cm^{-1}. The dispersed light was collected by a 1024 × 256 open electrode CCD detector. Confocal pinhole was set to 1000 μm. The depth resolution of this "true-confocal" configuration is usually better than 2 μm. Spectra were recorded unpolarized in scanning-mode [11]. All spectra were corrected for linear background and fitted to Gauss-Lorentz functions. Accuracy of Raman line

Table 1
Experimental conditions, data collection and refinement parameters

Radiation type, source	X-ray, Cu$K\alpha_1$
Generator settings	40 kV, 40 mA
Discriminator	Primary beam, curved Ge(111) monochromator
Detector	Linear PSD, 6° width
Effective μt	0.79
Data collection temperature	23.5(5) °C
Range in 2θ	4–100°
PSD step size	0.1°, 80 s/step
Internal integration step size	0.01°
a (Å)	11.13623(5)
c (Å)	21.9890(2)
V (Å^3)	2361.63(2)
Space group	$R3c$
Chemical formula	$K_{9.6}Ca_{1.2}Si_{12}O_{30}$
Z	3
D_{calc} (g cm^{-3})	2.617
No. of contributing reflections	465
No. of global parameters	1
No. of profile parameters	7
No. of intensity dependent parameters	35
R_p	16.0%
R_{wp}	14.3%
R_{Bragg}	6.73%
χ^2	1.66

shifts, calibrated by regular measuring the Rayleigh line, was in the order of $0.5\,cm^{-1}$.

3. Structure solution and refinement

A comparison with the previously reported X-ray powder diffraction pattern of $K_8CaSi_{10}O_{25}$ (PDF-4 entry 27-1026) based on the data of Gunawardane and Glasser [10] revealed the presence of several additional low-intensity lines in our diffractogram. There are at least two possible explanations for this result: (a) the powder pattern is more complex, i.e. weak reflections have been overlooked in the previous study and/or (b) the specimen contains impurities. In order to find a unit cell matching the powder pattern, the 2θ-positions of the first 29 lines were determined via the peak search algorithm implemented in the program FullProf.2k [12]. A first inspection of this list using the program TREOR90 [13] showed that the peaks could be indexed on the basis of a hexagonal R-centred unit cell with $a = 11.13\,Å$ and $c = 21.96\,Å$. The figures of merit M_{20} and F_{20} [14,15] for assessing the quality of this initial solution are $M_{20} = 34$ and $F_{20} = 52$ (0.005171, 75). This cell is related to the one reported in the earlier study mentioned above: whereas the a-axes are almost identical, the c-axis of our solution is doubled. The comparison of the LeBail fits obtained with the two cells shows clearly that the new metric provides a much better description of the observed powder pattern (see Fig. 1). A more detailed analysis of the systematic absences with the program CHECKCELL [16] pointed to the existence of a c-glide plane with $R\bar{3}c$ or $R3c$ as the most probable space groups. Extraction of the integral intensities as well as the structure solution by direct methods was accomplished using the EXPO program suite [17]. After subtraction of the background scattering, the integral intensities of reflections up to $2\theta = 80^\circ$ were obtained with Pearson VII profile functions. The final profile residual of this procedure converged to $R_{wp} = 12.3\%$. Both possible trigonal space groups, $R\bar{3}c$ and $R3c$, were tested for the structure determination. However, only in the non-centrosymmetric case a phase set and an E-map could be found, the most intense peaks of which could be interpreted as the atomic positions of a partial structure of a tetrahedral framework. In order to complete the structure model, a geometrically optimized network (program DLS-76 [18]) was introduced into the program SHELXL-93 [19]. Difference Fourier maps were calculated, clearly showing the positions of the missing non-tetrahedral K/Ca-positions. The structure refinements of the atomic parameters were initiated with the program FullProf.2k [12]. For Rietveld analysis, the background was determined by linear interpolation between consecutive breakpoints in the pattern. Intensities within seven times the full width at half maximum of a peak were considered to contribute to the central reflection. Thompson–Cox–Hastings pseudo-Voigt functions were chosen for the simulation of the peak shape, including an asymmetry

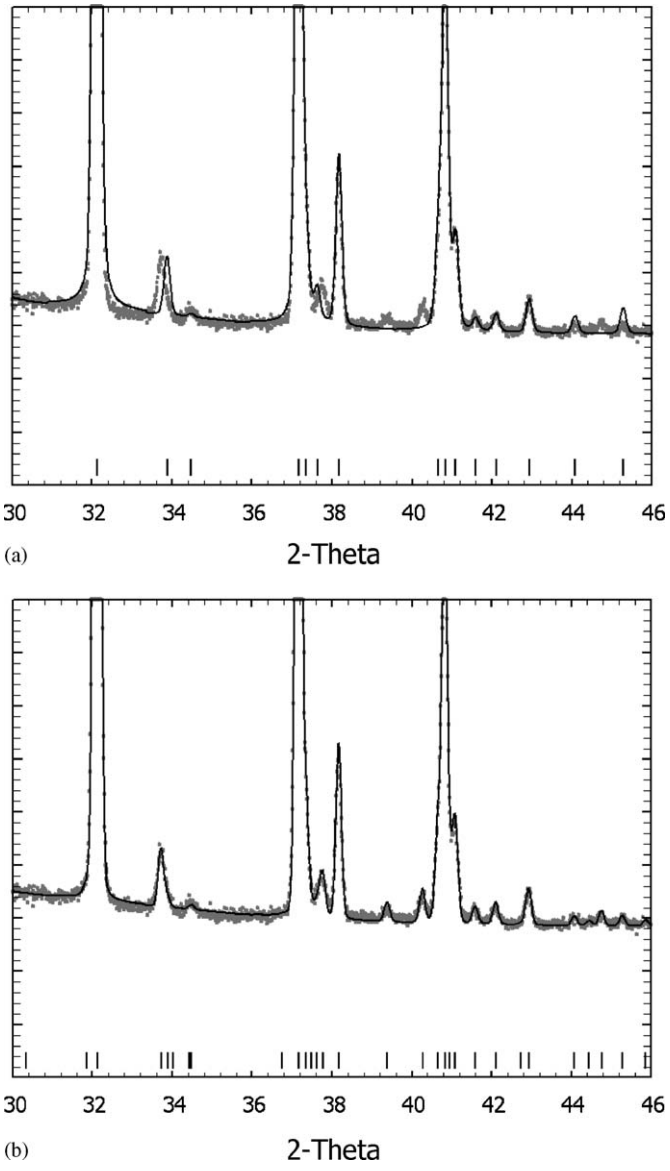

Fig. 1. Comparison between the structure-independent LeBail fits within a small part of the powder pattern: (a) "small" R-centred cell ($c = 10.98\,Å$) proposed by Gunawardane and Glasser [10], and (b) "large" R-centred cell with $c = 21.96\,Å$.

correction following Finger et al. [20]. The angular variation of the line width was accounted for by using the Caglioti function [21]. The refinement was done in consecutive steps with the atomic coordinates and thermal parameters held fixed in the initial calculations. They were allowed to vary after the scale factor, zero point, peak shape parameters and lattice constants were close to convergence to their optimum values. In order to avoid convergence problems, soft constraints for the Si–O and the O–Si–O bonds were applied assuming a Si–O distance of 1.62 Å, and a O–Si–O angle of 109.4°. A weight was given to these constraints by applying sigma values of 0.005 and 0.30 to the prescribed distances and angles, respectively. Si–O–Si angles have not been constrained in order to permit a more flexible orientation of the tetrahedra in the

framework structure. Due to the similar scattering power of the isoelectronic cations K^+ and Ca^{2+}, no attempts were made to tell them apart by mixed site scattering refinements. A graphical comparison between the observed and calculated powder pattern is given in Fig. 2. A final inspection of the structural model using the MISSYM subroutine of the program PLATON [22] revealed no indication for the choice of a space group of unnecessarily low symmetry. The refined fractional atomic coordinates are listed in Table 2 and selected interatomic distances and angles in Tables 3 and 4, respectively. According to Bérar and Lelann [23], a correction factor of 3.0 should be applied to the estimated standard deviations of the refined parameters. For drawing of structural details the program ATOMS [24] was employed. Bond valence calculations were based on the parameter sets given by Brese and O'Keeffe [25].

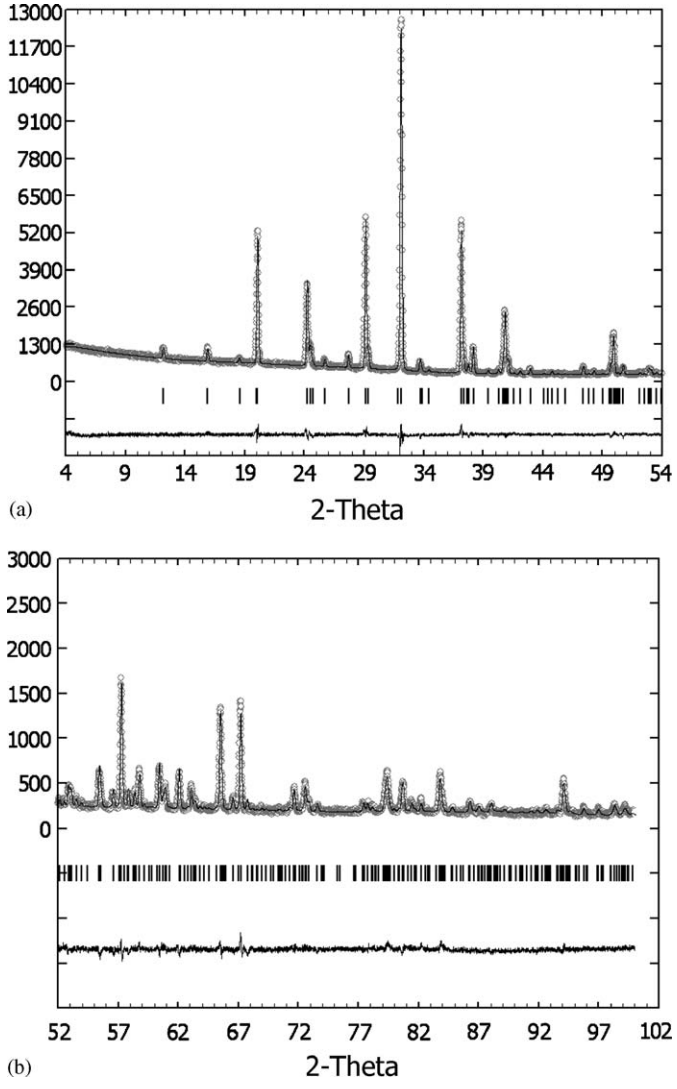

Fig. 2. Observed (circles) and calculated (solid line) step intensities and their difference (line at the bottom of figure) of $K_{9.6}Ca_{1.2}Si_{12}O_{30}$. Peak positions permitted by unit cell metric are indicated by tick marks (middle portion).

Table 2
Fractional atomic coordinates, isotropic displacement parameters ($Å^2$) and site occupancies

Atom	Wyckoff-site	x	y	z	B_{iso}	Occupancy
Si1	18(b)	0.4953(3)	−0.0226(3)	0.68034(14)	1.21(3)	1.0
Si2	18(b)	0.5098(3)	0.0141(3)	0.81871(15)	1.21(3)	1.0
*M*1	6(a)	0.33333	0.66667	0.91780	1.78(8)	0.60 Ca 0.40 K
M2A	18(b)	0.8350(10)	0.1627(9)	0.6394(4)	1.79(5)	0.605(9)
M2B	18(b)	0.8300(12)	0.1700(13)	0.6766(5)	1.79(5)	0.395(9)
*M*3	6(a)	0.33333	0.66667	0.7590(7)	1.79(5)	0.40
*M*4	6(a)	0.66667	0.33333	0.7425(3)	1.79(5)	1.0
O1	18(b)	0.5617(10)	0.1269(5)	0.6544(4)	2.60(7)	1.0
O2	18(b)	0.3330(4)	−0.1216(7)	0.6715(4)	2.60(7)	1.0
O3	18(b)	0.4428(8)	−0.4369(9)	0.8573(4)	2.60(7)	1.0
O4	18(b)	0.5401(6)	−0.0280(7)	0.75116(16)	2.60(7)	1.0
O5	18(b)	0.5670(9)	−0.0980(9)	0.6423(3)	2.60(7)	1.0

The sites *M*2–*M*4 are occupied by K only. *M*1 has a mixed Ca/K population. The partial occupancy of *M*3 refined to a value of 0.42(3). In this table it is adjusted to 0.40 to obtain a charge balanced structure.

Table 3
Selected interatomic distances (Å) up to 3.4 Å

Bond	Distance	Bond	Distance	Bond	Distance
Si1–O1	1.553(6)	*M2A*–O1	2.884(16)	*M2B*–O1	2.822(18)
Si1–O2	1.590(5)	*M2A*–O1	2.861(13)	*M2B*–O1	2.784(17)
Si1–O4	1.645(5)	*M2A*–O2	3.298(9)	*M2B*–O2	3.211(11)
Si1–O5	1.647(12)	M2*A*–O2	3.370(12)	*M2B*–O3	2.854(18)
Mean	1.609	*M2A*–O3	2.960(14)	*M2B*–O3	2.919(17)
Si2–O2	1.602(5)	*M2A*–O3	3.035(15)	*M2B*–O4	3.295(12)
Si2–O3	1.551(9)	*M2A*–O3	2.814(14)	*M2B*–O4	3.288(12)
Si2–O4	1.643(6)	*M2A*–O4	2.817(11)	*M2B*–O5	3.052(12)
Si2–O5	1.597(13)	*M2A*–O5	2.945(10)	*M2B*–O5	3.304(14)
Mean	1.598	*M*3–O2	3.045(13) × 3	*M*4–O1	2.778(8) × 3
*M*1–O3	2.448(11) × 3	*M*3–O3	2.982(15) × 3	*M*4–O2	3.161(9) × 3
*M*1–O1	2.516(7) × 3	*M*3–O4	3.011(6) × 3	*M*4–O5	2.993(8) × 3

Table 4
Selected bond angles (deg)

Bond	Angle	Bond	Angle
O1–Si1–O2	117.7(6)	O2–Si2–O3	115.0(6)
O1–Si1–O4	113.3(7)	O2–Si2–O4	98.7(5)
O1–Si1–O5	105.5(9)	O2–Si2–O5	107.9(9)
O2–Si1–O4	110.5(5)	O3–Si2–O4	107.6(7)
O2–Si1–O5	104.9(8)	O3–Si2–O5	118.1(11)
O4–Si1–O5	103.2(7)	O4–Si2–O5	107.5(9)
Mean	109.3	Mean	109.1
Si1–O2–Si2	159.3(4)	Si1–O4–Si2	137.4(4)
Si1–O5–Si2	141.7(7)		

4. Description of the crystal structure

In the crystal structure of $K_{9.6}Ca_{1.2}Si_{12}O_{30}$, silicate tetrahedra are linked into a three-dimensional framework with the stoichiometry $[Si_2O_5]^{2-}$, and a Si:O ratio of 1:2.5. Apart from the current phase, this Si:O ratio has been

observed only for a few other framework silicates, although it is known for many single layer, double chain and a few double ring silicates [26]. Basic building units of the framework are open branched *vierer* single chains (see Fig. 3) running parallel [211], (or the symmetry equivalent directions [$\bar{1}11$] and [$\bar{1}\bar{2}1$], respectively). The translation period of about 9.74 Å along these chains corresponds to the a_R lattice constant of the rhombohedral setting of $R3c$. A different understanding of the structure can be obtained by sub-dividing the framework into tetrahedral layers running parallel to (001) (see Fig. 4). A single 3.7 Å wide sheet contains isolated six-membered rings in UDUDUD conformation. Linkage between the rings of adjacent layers by common oxygen corners results in an ABCABC-type stacking sequence and consequently in the formation of a three-dimensionally connected network of tetrahedra.

In more detail, there are two crystallographically independent Si atoms, each of which is part of the network.

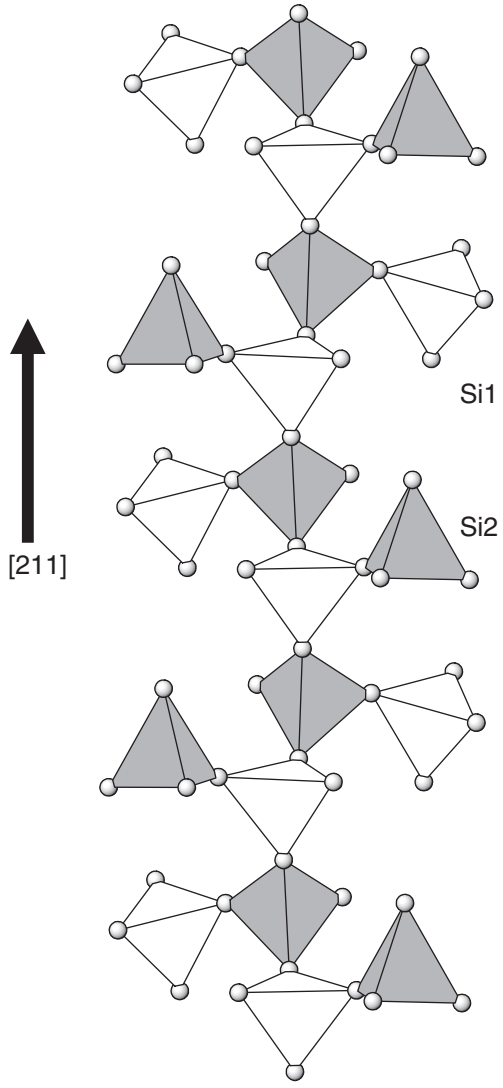

Fig. 3. Side view of a single open-branched *vierer*-chain in $K_{9.6}Ca_{1.2}Si_{12}O_{30}$. The two symmetrically independent tetrahedra are given in light- and medium gray.

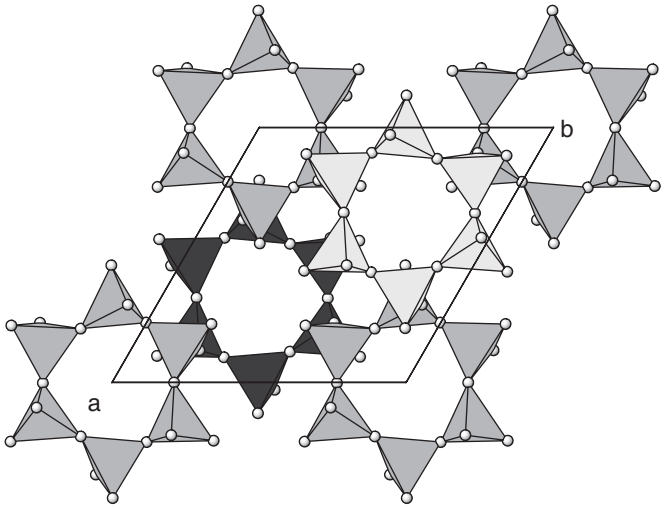

Fig. 4. Sequence of three adjacent layers parallel (001) containing isolated six-membered rings in UDUDUD conformation (tetrahedra in dark gray: $z \approx -0.167$; medium gray: $z \approx 0.00$; light gray: $z \approx 0.167$).

All SiO_4-tetrahedra have three bridging (br.) and one non-bridging (nbr.) vertex. This connectivity implies that the current potassium calcium silicate belongs structurally to the rare group of interrupted silicate frameworks with exclusively tertiary (Q^3) tetrahedral units. Concerning the individual Si–O bond distances, two groups can be distinguished: the Si–$O_{nbr.}$ bond lengths are significantly shorter (1.551–1.553 Å) than the Si–$O_{br.}$ bond distances (1.590–1.647 Å). This shortening results from the stronger attraction between O and Si than between O and K/Ca in the structure, and is a typical result for silicates containing Q^3 units. Whereas the average values of the O–Si–O angles for the two tetrahedra are very close to the ideal value of 109.47°, the individual O–Si–O angles range from 99° to 118°. This indicates that the tetrahedra deviate considerably from regularity. However, the scatter is similar to the values reported in the literature for other interrupted frameworks. The degree of distortion can be expressed numerically using the quadratic elongation λ and the angle variance σ^2 [27]. These parameters have values of $\lambda = 1.008$; $\sigma^2 = 32.2$ (for Si1) and $\lambda = 1.012$ and $\sigma^2 = 50.5$ (for Si2).

The Si–O–Si angles show a spread between 137° and 159° with an average of 146.1°. This mean value is about 6° higher than the value 140° corresponding to an unstrained Si–O–Si angle [26]. Bond valence sums (BVS) for the two Si atoms are close to the expected values: Si1: 4.19 and Si2: 4.31, respectively.

Charge compensation within the structure is achieved by the incorporation of potassium and calcium cations which are distributed among four crystallographically independent extra-framework sites. A careful analyses of the site occupancies during the refinements revealed that the positions $M1$ and $M4$ are fully occupied. The $M2$-site is split into two sites ($M2A$, $M2B$) only 0.83 Å apart from each other. For the final least squares refinements it was

assumed that the sum of the occupancy factors of both split positions is 1.0. It has to be pointed out that calculations performed without this constraint resulted in unstable refinements. The *M*3-position in turn is only partially occupied with an occupancy of 0.42(3). Split positions and partially occupied sites are not uncommon for extra-framework cations and have been observed in many zeolite-type structures, for example.

The coordination polyhedron about *M*1 can be described as a slightly distorted octahedron. For each of the remaining extra-framework cations, more complex polyhedra with nine oxygen ligands can be found in the range up to 3.4 Å. As can be seen from Fig. 5, the cation sites *M*1, *M*3 and *M*4 are located in tunnels formed within the network. These channels are running along [001] and are located around the 3-fold axes. Primarily, these three sites provide linkage between the tetrahedral rings of different layers. The *M*2-cations in turn are located on *z*-levels corresponding more or less to the mean plain of the rings and predominantly connect the rings within a single tetrahedral sheet.

Since the scattering powers of K^+ and Ca^{2+} are almost identical, the allocation of the different cation species to the *M*-sites was based on bond lengths considerations aided by the result from the chemical analysis. Typical Ca–O bond distances in calcium silicates, for example, have values in the range between 2.3 and 2.5 Å. Therefore, only *M*1 was considered to be a possible host site for the 3.6 calcium atoms which are present in the unit cell (according to the chemical analysis). On the other hand, the site scattering refinement indicated a full occupancy of *M*1, i.e. the remaining 2.4 atoms on this six-fold site were attributed to K, leaving a total of 26.4 positive charges per unit cell to be distributed among the positions *M*2–*M*4. According to the observed bond distances, these sites have to be exclusively occupied by potassium cations. In this regard, the partially occupied *M*3-site is of special interest. As mentioned above, the refinements resulted in an occupancy of 0.42(3) for this six-fold position, which corresponds to 2.52 positive charges per unit cell. Within one standard deviation, this refined parameter corresponds to the value of 0.40 (= 2.40 positive charges) that would be required to assure a charge balanced crystal. Therefore, in the final calculations the occupancy for *M*3 was fixed to the theoretical value. In summary one can say that the combination of information extracted from bond distance considerations, site occupancy refinements and chemical analysis results in a self-consistent structural model concerning charge neutrality and crystal chemistry. For the summary in Table 1 we preferred to describe the chemical formula of the present compound according to $K_{9.6}Ca_{1.2}Si_{12}O_{30}$, resulting in $Z = 3$ formula units per cell. The formula $K_8Ca_1Si_{10}O_{25}$ proposed by Gunawardane and Glasser [10], although leading to the same bulk composition, has the disadvantage that it is combined with a non-integral number of $Z = 3.6$.

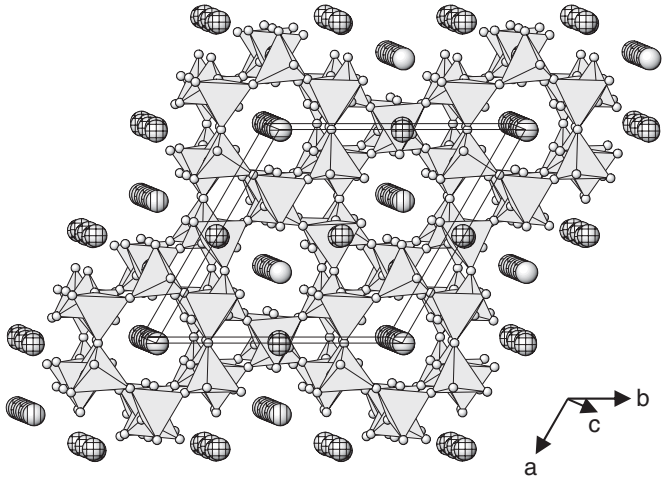

Fig. 5. Side view of the whole crystal structure of $K_{9.6}Ca_{1.2}Si_{12}O_{30}$. The different *M*-sites are represented by larger spheres (*M*1: no hatching; *M*2: cross-hatching; *M*3: horizontal hatching; *M*4: vertical hatching). The small spheres correspond to the oxygen anions.

5. Topological aspects

The framework density [28] of the present porous crystal structure is 15.2 T-atoms/1000 Å^3. This value is comparable with those observed in zeolite framework types like AEI or UTL, for example [29]. The connectivity of the T-atoms within the framework can be characterized by the so-called coordination sequences, which are identical for both silicon atoms in the asymmetric unit: 3-6-11-20-32-46-60-80-102-122. The vertex symbols for the two tetrahedral centers are $10_2 \cdot 10_2 \cdot 6_1$ (see Fig. 6). Concerning the topology, the interrupted framework in $K_{9.6}Ca_{1.2}Si_{12}O_{30}$ can be classified as a three-dimensional 3-connected net. A detailed theoretical treatment of these net types has been given by Wells [30]. Actually, the net observed in the present structure has been already noted in his comprehensive listing. The maximal topological space group symmetry of this framework type is $R\bar{3}m$. It belongs to the so-called Archimedean 3-connected nets, indicating that at least two of the shortest circuits meeting at each vertex are of different kinds concerning the number of points belonging to the rings.

Most of the known interrupted tetrahedral frameworks correspond to unbroken parent frameworks that are observed in other structures. The construction of the theoretical parent framework is useful in order to show structural relationships and to predict possible framework configurations. The theoretical parent framework structure was constructed from the present network by inserting two additional T-atoms at the positions (0,0,2/3) and (0,0,1/3). Interestingly, the resulting three-dimensional 4-connected net is one of the most important in inorganic chemistry. It can be found in the diamond structure or in cristobalite, for example (see Fig. 7). Therefore, the tetrahedral net observed in $K_{9.6}Ca_{1.2}Si_{12}O_{30}$ can be described as a defect

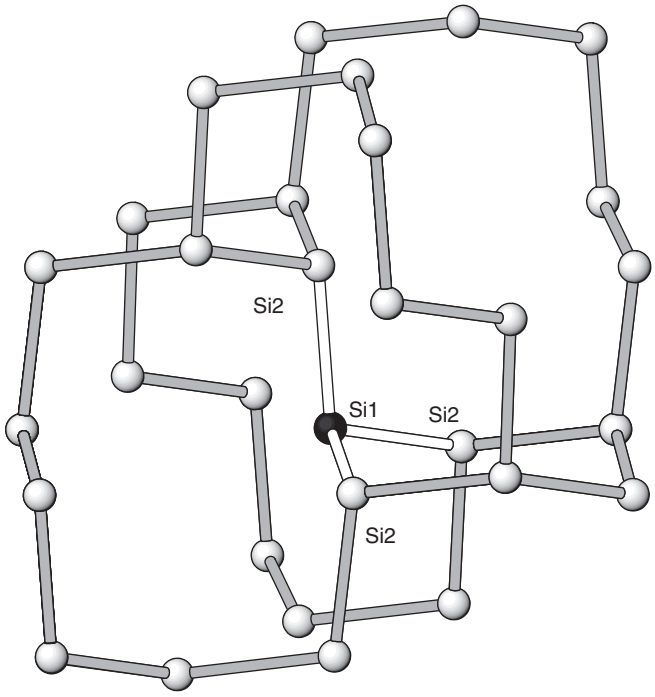

Fig. 6. Graphical representation of the vertex symbol $10_2 \cdot 10_2 \cdot 6_1$ observed for Si1 in $K_{9.6}Ca_{1.2}Si_{12}O_{30}$.

cristobalite net where 20% of the tetrahedral centers have been removed.

6. Raman spectroscopy

The Raman spectrum of polycrystalline $K_{9.6}Ca_{1.2}Si_{12}O_{30}$ is displayed in Fig. 8. Total of 21 bands from 125 to 1138 cm^{-1} with a range of full width at half maximum of 7–77 cm^{-1} could be detected (Table 5, Fig. 8). Relative intensities, normalized to the highest intensity band at 548 cm^{-1}, vary between 2% and 89%. Neglecting differences between *M*2A and *M*2B a simplified factor group analysis yields in total 135 Raman- and IR-active vibrational modes:

$$\Gamma_{vib} = 27A_1 + 54E.$$

Since 54 vibrations are doubly degenerated *E*-modes, the total number of observed bands in the spectrum reduces significantly. Raman-active bands of alkali and alkaline earth metal silicates in the wavenumber range 850–1250 cm^{-1} can be assigned to symmetric $Si–O^-$ stretching vibrations of SiO_4 groups with non-bridging oxygens [$\nu_s(Si–O^-)$] [31,32]. Bands between 400 and 800 cm^{-1} are generally symmetric bending vibrations of the Si–O–Si bridging oxygens [δ_s(Si–O–Si)], which reflect the connectivity between adjacent silicon–oxygen tetrahedra. Quantum chemical calculations with silicon–sodium tetrahedral model clusters revealed a negative correlation for the Si–O–Si angles in the range of 115–165° and the δ_s(Si–O–Si) in the wavenumber range of 900–400 cm^{-1} [32].

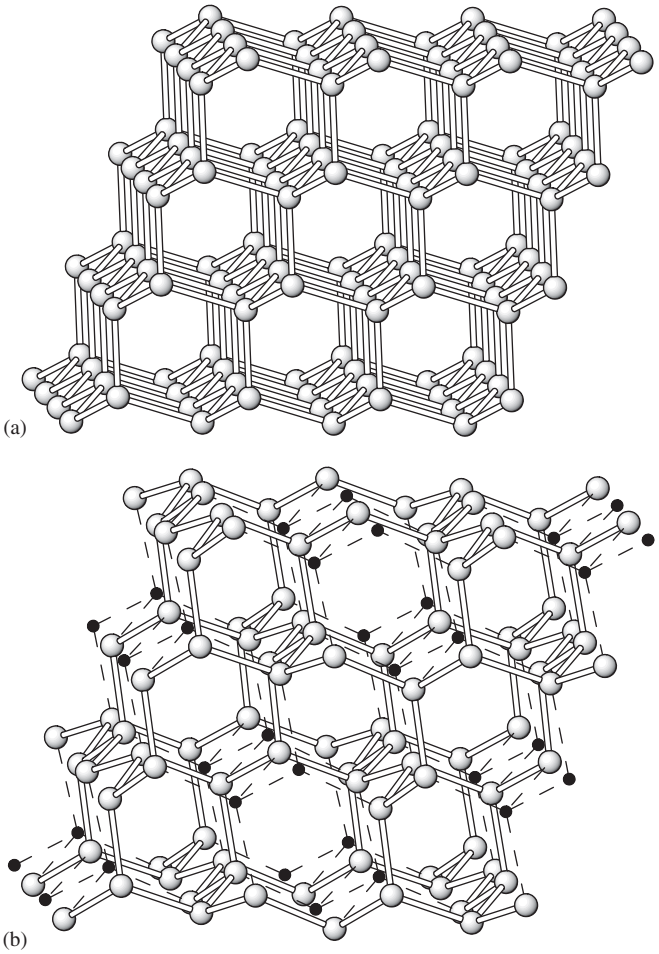

Fig. 7. Comparison between the topology of the nets observed in (a) diamond and (b) the parent framework of $K_{9.6}Ca_{1.2}Si_{12}O_{30}$. The dark spheres correspond to the additional T-atoms in (0,0,1/3) and (0,0,2/3) inserted to construct the 4-connected net. The resulting new bonds (thin dashed lines) have been added as a guide for the eyes.

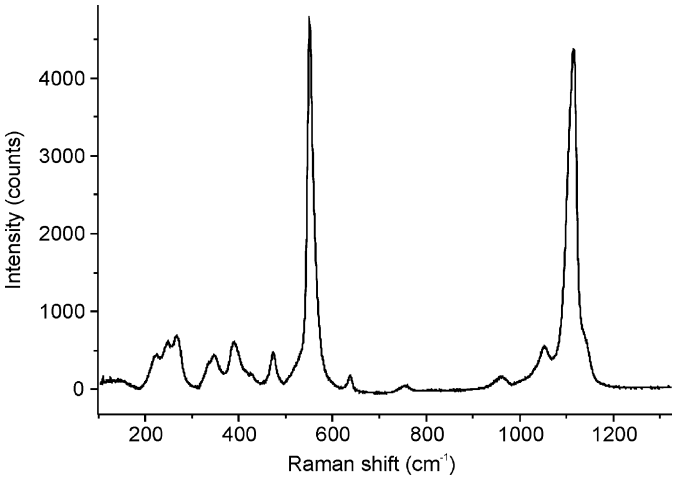

Fig. 8. Raman spectrum of polycrystalline $K_{9.6}Ca_{1.2}Si_{12}O_{30}$.

According to You et al. [32], Si–O–Si angles between 137 and 159°, which have been determined in $K_{9.6}Ca_{1.2}Si_{12}O_{30}$, would correspond to δ_s(Si–O–Si) bands at 610–490 cm^{-1},

Table 5
Shifts (in cm^{-1}), relative intensities and assignment of the Raman bands observed in $K_{9.6}Ca_{1.2}Si_{12}O_{30}$ polycrystalline sample

$K_{9.6}Ca_{1.2}Si_{12}O_{30}$ (this study)	Relative intensities[a]	Assignment
125	5	(K–,Ca–O), phonons
216	9	(K–,Ca–O), phonons
244	17	(K–,Ca–O), phonons
266	14	(K–,Ca–O), phonons
329	3	(K–,Ca–O), phonons
344	12	(K–,Ca–O), phonons
386	14	(K–,Ca–O), phonons
402	6	δ_s(Si–O–Si)
425	3	δ_s(Si–O–Si)
471	13	δ_s(Si–O–Si)
528	6	δ_s(Si–O–Si)
548	100	δ_s(Si–O–Si)
557	50	δ_s(Si–O–Si)
635	4	δ_s(Si–O–Si)
755	2	δ_s(Si–O–Si)
957	3	ν_s(Si–O^-)
1051	7	ν_s(Si–O^-)
1066	7	ν_s(Si–O^-)
1108	89	ν_s(Si–O^-)
1116	56	ν_s(Si–O^-)
1138	12	ν_s(Si–O^-)

[a]In % of the most intense band at 548 cm^{-1}.

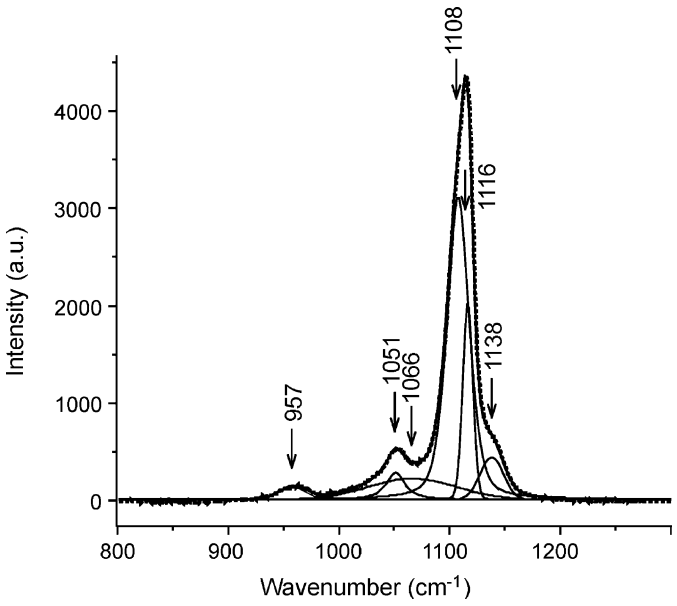

Fig. 9. Deconvolution of the high-wavenumber range of $K_{9.6}Ca_{1.2}Si_{12}O_{30}$. Dots indicate the recorded spectrum, thin and thick solid lines represent deconvoluted peaks and band sum, respectively.

in agreement to experimentally observed high intensity bands (635–471 cm^{-1}) in the middle wavenumber range (Table 5). Bands at lower (402, 425) and higher (755) wavenumbers maybe explained by further factors affecting the vibrational wavenumber of δ_s(Si–O–Si) like connectivity of Si-tetrahedra and/or impacts of the non-framework cations [32].

In the wavenumber range below 400 cm^{-1}, bands are caused by lattice vibrations of the skeleton framework as well as the bonding interactions between the non-framework cations and oxygen (K–O, Ca–O). Previous studies [32–34] suggested that the Raman shift of the symmetric Si–O stretching modes above 850 cm^{-1} in silicates is related to the structure of the Q^x tetrahedral units (x = number of the bridging oxygens of the tetrahedral unit). Deconvolution of this part of the spectrum of $K_{9.6}Ca_{1.2}Si_{12}O_{30}$ yielded six bands at 957, 1051, 1066, 1108 1116 and 1138 cm^{-1} (Fig. 9). Raman peaks of ν_s(Si–O^-) vibrations of six-membered rings linked to Q^3-connected sheets of silicon tetrahedra in Na_2O–$2SiO_2$ crystals were experimentally recorded at 1072 and 1079 cm^{-1}, respectively [32,35]. According to theoretical calculations performed on clusters of silicon tetrahedra in binary sodium silicates, bands at wavenumbers above 1032 cm^{-1} correspond to Q^3 species linked in up to three hexagonal rings [32]. The most intense Raman bands of $K_{9.6}Ca_{1.2}Si_{12}O_{30}$ in the high-wavenumber range at 1108 and 1116 cm^{-1} thus suggest a dominating superstructure arrangement of Q^3 units in six-membered hexagonal rings, which is consistent to the findings of the structure refinement.

7. Concluding remarks

Concerning the crystal chemistry, the structure of $K_{9.6}Ca_{1.2}Si_{12}O_{30}$ is rather an exception. Although several thousand crystal structures of natural and synthetic silicates have been determined, there are only a few interrupted frameworks known which are exclusively based on tertiary (Q^3)-tetrahedra. A compilation of these materials studied so far can be found in a recent paper on the crystal structure of γ-$Na_2Si_2O_5$ [36]. Apart from being a structural curiosity, compounds such as γ-$Na_2Si_2O_5$ or $K_{9.6}Ca_{1.2}Si_{12}O_{30}$ could be of special interest in glass science. According to Zachariasen's classical theory, the internal structure of a glass can be described with a random network model [37 and references cited in there]. For alkali and alkaline earth silicate glasses this approach has been interpreted in such a way that the alkaline earth and alkali cations occupy the interstitial space of the tetrahedral network and behave as so-called network modifiers, creating non-bridging oxygens. For silicate glasses with a Si:O ratio of 1:2.5, for example, one should expect a tetrahedral network that is dominated by the presence of Q^3-units. However, looking at the crystalline analogues in these systems having the same Si:O ratio it has to be stated that the vast majority are layered compounds. Only the interrupted frameworks have a similar but, of course, translationally ordered network structure. They could provide models for a better understanding of the arrangement of the tetrahedra and network modifiers in silicate glasses.

The existence of a framework structure with extra-framework cations on interstitial sites offers the possibility of a flexible chemical composition, i.e. the formation of

solid solutions is likely to occur. For example, the exclusive occupation of the *M*1-site with Ca combined with a completely vacant *M*3-site would result in a charge balanced framework structure with composition $K_8Ca_2Si_{12}O_{30}$. On the other hand, full occupancy of all four *M*-sites with potassium would lead to a structure with composition $K_{12}Si_{12}O_{30}$ (or $K_2Si_2O_5$). Actually, the existence of such a type of pure potassium disilicate has been recently reported [38]. The structure determination based on a single crystal data set collected at 150 K indicated that the symmetry of this $K_2Si_2O_5$-phase is no longer trigonal, but monoclinic (space group *Cc*, a sub-group of index 3 of *R*3*c*). However, a critical review of the observed bond distances in the monoclinic disilicate shows clearly that the K–O bond distances for several extra-framework sites are much lower compared to the values usually observed in silicate structures. Since the authors did not provide a chemical analysis it cannot be excluded that the structurally related "pure" potassium disilicate may have been stabilized by the incorporation of impurities. In summary one can say that a solid solution series of the type $K_{8+2x}Ca_{2-x}Si_{12}O_{30}$ probably exists although it may be limited to *x*-values significantly lower than 2.0. Within this hypothetical series the present compound would represent a point with $x = 0.8$.

References

[1] Z. Qian, T.L. Tolt, A.R. Cooper, J. Am. Ceram. Soc. 70 (1987) 48–53.
[2] K.H. Wedepohl, Glastech. Ber. 70 (1997) 246–255.
[3] K. Gerth, K.H. Wedepohl, K. Heide, Chem. Erde—Geochem. 58 (1998) 219–232.
[4] W.B. Stern, Y. Gerber, Archaeometry 46 (2004) 137–156.
[5] H. Hughes, Trans. Brit. Ceram. Soc. 65 (1966) 661–679.
[6] P. Thy, B.M. Jenkins, C.E. Lesher, Energ. Fuel. 13 (1999) 839–850.
[7] J.L. Jorda, S. Prokic, L.B. McCusker, C. Baerlocher, C.F. Xue, J.X. Jong, Comp. Rend. Chim. 8 (2005) 331–339.
[8] W.C. Taylor, J. Res. Natl. Bur. Stand. 27 (1941) 311–323.
[9] G.W. Morey, F.C. Kracek, N.L. Bowen, J. Soc. Glass Technol. 14 (1930) 149–187.
[10] R.P. Gunawardane, F.P. Glasser, Z. Anorg. Allg. Chem. 411 (1975) 163–171.
[11] P. Knoll, R. Singer, W. Kiefer, Appl. Spectrosc. 44 (1990) 776–782.
[12] J. Rodriguez-Carvajal, FullProf.2k, version 3.3, Laboratoire Leon Brillouin (CEA-CNRS), France, 2005.
[13] P.E. Werner, L. Eriksson, M. Westdahl, J. Appl. Crystallogr. 18 (1985) 367–370.
[14] P.M. De Wolff, J. Appl. Crystallogr. 1 (1968) 108–113.
[15] G.S. Smith, R.L. Snyder, J. Appl. Crystallogr. 12 (1979) 60–65.
[16] J. Laugier, B. Bochu, CHECKCELL. Laboratoire des Matériaux et du Génie Physique, Ecole Nationale Supérieure de Physique de Grenoble (INPG) Domaine Universitaire BP 46, 38402 Saint Martin d'Hères. France, 2000.
[17] A. Altomare, M.C. Burla, M. Camalli, B. Carrozzini, C. Giacovazzo, A. Guagliardi, A.G.G. Molitierni, G. Polidori, R.J. Rizzi, J. Appl. Crystallogr. 32 (1999) 339–340.
[18] C. Baerlocher, A. Hepp, W.M. Meier, DLS-76, Institut für Kristallographie und Petrologie, ETH Zürich, Switzerland, 1977.
[19] G.M. Sheldrick, SHELXL-93, Program for the refinement of crystal structures, Universität Göttingen, Germany, 1993.
[20] L.W. Finger, D.E. Cox, A.P. Jephcoat, J. Appl. Crystallogr. 27 (1994) 892–900.
[21] G. Caglioti, A. Paoletti, F.P. Ricci, Nucl. Instrum. 3 (1958) 223.
[22] A.L. Spek, PLATON, A Multipurpose Crystallographic Tool, University of Utrecht, The Netherlands, 1998.
[23] J.F. Bérar, P.J. Lelann, J. Appl. Crystallogr. 24 (1991) 1–5.
[24] E. Dowty, ATOMS, Version 5.1, Shape Software, Kingsport, USA, 2000.
[25] N.E. Brese, M. O'Keeffe, Acta Crystallogr. B 47 (1991) 192–197.
[26] F. Liebau, Structural Chemistry of Silicates, Verlag, Berlin, 1985.
[27] K. Robinson, G.V. Gibbs, P.H. Ribbe, Science 172 (1971) 567.
[28] G.O. Brunner, W.M. Meier, Nature 337 (1989) 146.
[29] Ch. Baerlocher, W.M. Meier, D.H. Olson, Atlas of Zeolite Framework Types, fifth revised ed., Elsevier, Amsterdam, 2001.
[30] A.F. Wells, Further studies of three-dimensional nets. American Crystallographic Association Monographs No. 8, 1979.
[31] M.E. Fleet, G.S. Henderson, Phys. Chem. Minerals 24 (1997) 345–355.
[32] J.-L. You, G.-C. Jiang, H.-Y. Hou, H. Chen, Y.-Q. Wu, K.-D. Xu, J. Raman Spectrosc. 36 (2005) 237–249.
[33] S.K. Sharma, T.C. Hoering, H.S. Yoder Jr., Year Book—Carnegie Institution of Washington 78 (1979) 537–542.
[34] M. Akaogi, N.L. Ross, P. McMillan, A. Navrotsky, Am. Mineral. 69 (1984) 499–512.
[35] A.M. Efimov, J. Non-Cryst. Solids 253 (1999) 95–118.
[36] V. Kahlenberg, S. Rakić, C. Weidenthaler, Z. Kristallogr. 218 (2003) 421–431.
[37] A.K. Varshneya, Fundamentals of Inorganic Glasses, Academic Press Inc., San Diego, 1994.
[38] B.H.W.S. deJong, H.T.J. Supèr, A.L. Spek, N. Veldman, G. Nachtegaal, J.C. Fischer, Acta Crystallogr. B 54 (1998) 568–577.